ELSEVIER

Journal of Fluids and Structures 19 (2004) 1061–1083

JOURNAL OF FLUIDS AND STRUCTURES

www.elsevier.nl/locate/jnlabr/yjfls

Flow-induced vibration of elastic slender structures in a cylinder wake

Y.L. Lau, R.M.C. So*, R.C.K. Leung

Department of Mechanical Engineering, The Hong Kong Polytechnic University, Hung Hom, Kowloon, Hong Kong, China

Received 14 March 2003; accepted 28 June 2004
Available online 14 October

Abstract

Flow-induced vibration of an elastic airfoil due to the wake propagating from an upstream cylinder at a Reynolds number of 10 000 based on cylinder diameter D was investigated. A laser vibrometer was employed to measure the bending and torsional vibration displacements at the mid-span of the airfoil and the cylinder. The dimensionless gap size S/D between the two structures was selected as the governing parameter of the flow-induced vibration problem. It is found that the vibration amplitudes of the elastic airfoil and the vortex shedding frequency of the coupled cylinder–airfoil system are strongly dependent on S/D, due to the different fluid–structure interaction experienced by the airfoil at various S/D. Strong vortex-induced vibration of the airfoil appears to be excited by the organized Karman-vortex-street (KVS) vortices in the cylinder wake for $S/D > 3$ and becomes stabilized for $S/D \leqslant 3$. However, as a result of the shear-layer-induced vibration at an appropriate frequency, structural resonance is also found to occur even though the airfoil is located in the stabilizing range. The occurrence of structural resonance is further supported by a complementary experiment where the slender structure is an elastic flat plate. This phenomenon indicates that assuming the structures in any fluid–structure interaction problem to be rigid is not appropriate, even though they might appear to be *highly* stiff. The experimental results were used to validate a numerical model previously developed to estimate the structural responses in complicated fluid–structure interaction problems.

1. Introduction

Among various combinations of two structures with different bluffness in different arrangements in a cross-flow, the most interesting one is that involving an upstream bluff body in tandem with a thin slender structure, because the presence of the slender structure is capable of influencing the aerodynamics and possibly stabilizing the unsteady forces acting on the upstream bluff body. If the bluff body is a circular cylinder, alternating vortices in a Karman-vortex-street (KVS) pattern are formed and shed as a result of boundary layer roll-up. They continue to grow under continuous injection of circulation from the cylinder shear layers until they become strong enough to draw the shear layers across the wake (Gerrard, 1966). The vortices stop building up their strength and shed away from the cylinder as the approach of vorticity with an opposite sign in sufficient concentration cuts off further supply of circulation to the forming vortex. The reduced frequency of vortex shedding, or Strouhal number $\mathrm{St} = f_s D/U_\infty$, has been studied over a broad range of $\mathrm{Re} = U_\infty D/\nu$ from approximately 50 to 10^6 and even higher (Zdravkovich, 1997), whereas the mechanics of vortex

*Corresponding author. Fax: +852 2365 4703.
E-mail address: mmmcso@polyu.edu.hk (R.M.C. So).

0889-9746/$ - see front matter © 2004 Elsevier Ltd. All rights reserved.
doi:10.1016/j.jfluidstructs.2004.06.007

formation has been closely examined by other researchers using various experimental techniques, e.g., Gerrard (1966), Perry et al. (1982), Nakagawa (1986), etc. Here, U_∞ is the free stream velocity, f_s is the vortex shedding frequency and v is the fluid kinematic viscosity. It is generally agreed that the vortex formation region plays an important role in vortex shedding and its f_s.

When a rigid splitter plate is placed in the wake of a circular cylinder, Roshko (1955), Nakagawa (1988), and Unal and Rockwell (1988) found that the normalized gap distance (S/D) between the leading edge of the splitter plate and the base of the cylinder in the stream direction has a notable influence on the wake evolution of the cylinder. As the plate is moved upstream towards the cylinder, it would modify the cylinder wake behavior in the vortex formation region into two different states, depending on S/D. Based on the influence of the splitter plate on the cylinder wake evolution, Roshko (1955) defined two vortex formation regimes; one is the pre-vortex formation regime whose length is defined as the downstream distance from the cylinder base at which irrotational fluid is drawn across the centerline, another is the post-vortex formation regime where the primary vortices form and develop fully while convecting downstream. When the splitter plate moves away from the post-vortex formation regime into the fully developed vortex formation regime far downstream, it does not have any notable effect on the characteristics of the wake propagated from the cylinder and the formation of the KVS vortices. At the moment the leading edge of the splitter plate is moved close to the boundary between the pre- and post-vortex formation regime, around $S/D=3$, it could affect the adjacent distance between the two rows of vortices in the KVS. When the plate approaches the cylinder base, the vortex formation mechanism of the cylinder wake is significantly altered. As a result, the vortices are shed behind the two structures (i.e., behind the splitter plate) and the wake develops as if the two structures had become an elongated combined structure.

Modification of the wake by downstream slender structures is not limited to a circular cylinder in a cross-flow. It takes place with cylinders of different cross-sectional shapes. Ozono (1999) examined a cylinder–plate interaction in a cross-flow with different cylinder shapes. He found that the variation of the base pressure and St of the cylinder with S/D were functions of Re, the transverse distance between the structures, and the shape of the cylinder itself. Hasan and Budair (1994) experimentally investigated the fluid–structure interaction of a coupled square cylinder–plate system over a Re range of 1.2×10^4–2.4×10^4, based on the side-length of the square cylinder. They found that the base pressure of the square cylinder, and the vortex shedding frequencies of the square cylinder alone, as well as the coupled cylinder–plate system are functions of the gap size between the structures, Re, the angle of attack of the square cylinder, and the ratio of the downstream plate length to the side length of the square cylinder. Mansingh and Oosthuizen (1990) experimentally studied the wake behind a rectangular cylinder with a downstream splitter plate at a Re varying from 0.35×10^3–1.15×10^3, and assessed the effects of the length of the splitter plate. They found that the splitter plate-altered vortex formation, caused a reduction in f_s, and gave rise to a reduction in the overall drag by up to 50%.

The fluid–structure interaction of a bluff body and a slender structure in tandem has also been investigated numerically. Arai and Komatsu (1992) used a Marker and Cell (MAC) method to examine the effects of S/D on the fluctuating lift- and drag-induced dynamic response of a square cylinder with a downstream plate. In their study, Re based on the side length of the square cylinder was set at 10 000. They found that by placing the plate at a suitable position downstream, the peak value of the fluctuating lift of the cylinder could be reduced to 40% of the isolated case. Lin and Wu (1994) employed an upwind finite volume method to investigate the influence of the presence of a downstream thin plate on the aerodynamic response of the upstream circular cylinder and the evolution of the wake shed behind the cylinder. In their investigation, the flow condition was set at $\mathrm{Re}=100$. They found that when $S/D<3$, the fluctuating lift and drag force of the cylinder could be reduced and there was no vortex shedding behind the cylinder. When $S/D>4$, the fluctuating aerodynamic response was not reduced and the downstream plate could not inhibit vortex shedding behind the cylinder. The downstream plate could destabilize the flow though.

The structural properties of the upstream bluff bodies and the downstream slender structures were assumed to be rigid in the above studies. Consequently, these studies only provided the changes in aerodynamic response and wake evolution due to the interaction of two structures in various spatial arrangements. In reality, all structures are to different degrees elastic, even though their stiffness might differ by several orders of magnitude. Therefore, it is important to consider the effects of a vibrating structure on the wake flow and, in turn, the effects of the modified wake flow on the vibrating structure.

Flow-induced vibration of an elastic cylinder with a rigid downstream slender plate has been reported in a number of studies. Kawai (1990) employed a discrete vortex method to investigate the structural dynamic response of an elastic circular cylinder in a cylinder–plate system by varying S/D. He found that as the upstream cylinder approaches resonant self-excitation, i.e., when the free-stream velocity is equal to its own reduced velocity, the downstream plate was able to reduce the amplitude level of the resonant vibration, as long as $S/D<1$. Nakamura and Tomonari (1977) and Nakamura et al. (1994) found that the downstream splitter plate might cause the upstream elastic cylinder to gallop, irrespective of its cross-sectional geometry.

Other investigations on similar fluid–structure interaction problems have been focusing on the possible controlling action of a downstream plate on the aerodynamic response of the upstream body and the evolution of its wake. However, the interaction between the modified wake and the downstream plate received little or no attention. The numerical studies of So et al. (1999), and Leung and So (2001) showed that, under excitation of an oncoming KVS, a rigid slender streamlined structure, be it an airfoil or a turbine blade, would exhibit aerodynamic resonance at which the aerodynamic response and sound generation are the highest. In addition, structural resonance would occur if the elasticity of the structure was taken into consideration. This fluid–structure resonant behavior is mainly characterized by the normalized frequency parameter c/d of the KVS, where c is the chord length of the slender structure and d is the streamwise separation between two adjacent vortices in the same row. Aerodynamic resonance occurs at distinct $c/d = 0.5$, 1.5, 2.5, etc. and is of pure aerodynamic origin. Taking structural elastic behavior into account, due to the coupling effects of fluid–structure interaction, as c/d approaches the normalized natural frequency of the airfoil/blade in still fluid, structural resonance also occurs. Therefore, it shows that the influence of the modified wake on the downstream airfoil/plate structural dynamics should not be neglected in an investigation of the coupled interaction of a bluff body and a slender structure, with either the slender structure or both being elastic.

The present study aims to extend the scope of the coupled interaction of two structures in a cross-flow and to fill the gap in similar investigations attempted previously. An experimental investigation on the flow-induced vibration of a relatively rigid circular cylinder and an elastic downstream slender airfoil was carried out using a laser vibrometer to measure the vibration transverse displacements of the structures and a particle image velocimetry (PIV) technique to measure the flow field. The S/D was varied in order to reveal the essential physics (i) of the interaction between the modified cylinder wake and the elastic airfoil, (ii) of the effect of a downstream vibrating airfoil on the unsteady loading of the upstream cylinder, and (iii) of the aerodynamic and structural response of both structures. In addition, the data thus obtained was used to verify a boundary element method (BEM) developed to simulate the interaction between oncoming KVS and a downstream elastic structure, such as that found in a rotor–stator pair of an axial flow turbomachine.

2. Experimental Apparatus

2.1. Wind tunnel setup

Experiments were carried out in a closed circuit wind tunnel having a test-section that is 2.3 m long and a square (0.6 m × 0.6 m) cross-section. The turbulent intensity of the flow entering the test-section was about 0.025%. The free-stream velocity U_∞ in the experiment was set at 5.48 m/s and the corresponding Reynolds number (Re) was estimated to be $\mathrm{Re} \approx 10\,000$. The experimental setup is schematically illustrated in Fig. 1. Details of the experimental and measurement setups are fully described below and in Lau (2003). A circular cylinder was vertically mounted in the mid-plane of the test-section at 0.2 m downstream of the exit plane of the contraction. A slender NACA0012 airfoil was placed downstream of the cylinder. The airfoil could be moved along the line joining its chord and the center of the upstream cylinder. The mountings of the cylinder and the airfoil were designed to provide fixed–fixed support at both

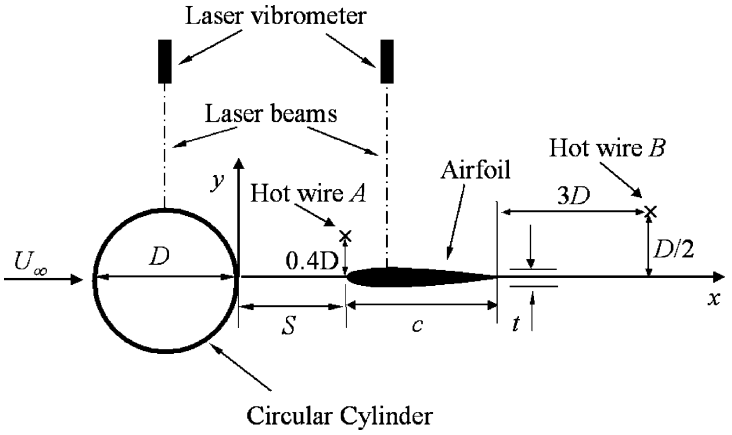

Fig. 1. Schematic of the experimental setup.

ends of the structures so that torsional and bending deflections at the support were negligible. The origin of the coordinate system was attached to the base of the cylinder at mid-span. The structural properties of the circular cylinder and the airfoil are listed in Table 1, where the damping ratio and natural frequencies of the structures were measured from impact test conducted in still air. It can be seen that the cylinder stiffness is three orders of magnitude larger than that of the airfoil. Therefore, the transverse flow-induced vibration amplitude of the cylinder is expected to be much smaller compared to that of the airfoil.

A detailed analysis of the effect of wind tunnel wall vibration on the structural vibration measurements has previously been reported in So et al. (2000). Therefore, this will not be repeated here, other than the salient points presented below. The vibration of the wind tunnel wall at the region near the mounting of the structures was monitored by one single laser beam of the Polytec Series 3000 Dual Beam Laser Vibrometer (Fig. 1). The output signal from the laser vibrometer was fed to a spectrum analyzer at a sampling frequency of 1.4 kHz. The final spectrum was constructed from the data by taking the average of 10 spectra recorded within 120 s. Fig. 2 shows a dominant frequency of 15.2 Hz in the wind tunnel wall vibration spectrum. From the spectral analysis of the vibration response of the structures (Section 3.6), it was found that the wind tunnel wall vibration frequency did not coincide with any frequency component of the vibration response of the cylinder and the airfoil. In addition, the root-mean-square (r.m.s.) value of the tunnel wall transverse vibration amplitude normalized by D, $(y_w/D)_{\mathrm{rms}}$, is 1×10^{-6}, which was at least 10 times less than the r.m.s. value of the weakest cylinder vibration response at $S/D = 3$ in the coupled cylinder–airfoil system. This

Table 1
Structural properties of the cylinder and the airfoil in the cylinder/airfoil system

Quantity	Circular cylinder	Airfoil (NACA0012)
Dimension (mm)	Outer diameter $D = 30$	Chord length $c = 30$
Span b (m)	0.6	0.6
Material	Brass	Aluminum
Mass/unit length (kg/m)	6.02	0.22
Bending stiffness/unit span k_Y (N/m^2)	1.37×107	1.76×104
Bending natural frequency in still air f_Y (Hz)	240 (First mode)	45.4 (First mode)
Torsion stiffness/unit span k_θ (N)	—	181.73
Torsion natural frequency in still air f_θ (Hz)	—	652.87
Mass ratio $M^* = m/\rho_{\mathrm{air}}D^2b$	5574.1	203.7
Reduced velocity $U_r = U_\infty/f_Y D$	0.76	4.02
Nondimensional bending natural frequency $f_Y D/U_\infty$	1.313	0.248
Nondimensional torsion natural frequency $f_\theta D/U_\infty$	—	3.574

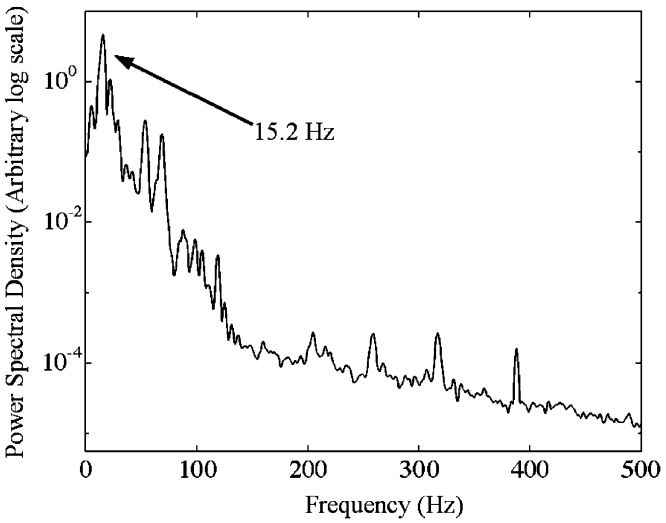

Fig. 2. Wind tunnel wall vibration spectrum.

indicates that the influence of the relatively weak tunnel wall vibration on the vibration behavior of the structures could be neglected.

2.2. Airfoil and cylinder models

The aluminum airfoil model with a NACA0012 profile was positioned at zero angle of attack with respect to the x-axis downstream of the cylinder. Its chord length c and span b_a were 0.03 and 0.6 m, respectively. Its centroid and shear center measured from the leading edge of the airfoil were located at 42% and 37% chord, respectively. The mass ratio of the airfoil was calculated to be $M_a^* = m_a/\rho_{\text{air}}D^2b_a = 203.7$, where m_a is the mass of the airfoil and ρ_{air} is the air density. The natural frequencies of the first bending and torsion vibration mode of the airfoil in still air were measured at 45.4 and 652.87 Hz, respectively.

The brass circular cylinder has a diameter $D = 0.03$ m and a span of 0.6 m (Table 1). Its reduced velocity $U_r = U_\infty/(f_{YI})_c D$ was 0.76, and the mass ratio was $M_c^* = m_c/\rho_{\text{air}}D^2b_c = 5574.1$, where $(f_{YI})_c$ was the first bending natural frequency of the cylinder in still air and m_c is the mass of the cylinder. If a two-degree-of-freedom (2-dof) structural dynamics model was assumed for the cylinder which was allowed to vibrate freely in the streamwise (x) and transverse (y) direction, it can be shown that the normalized equations of motion would lead to negligibly small displacement amplitude when the mass ratio was large and U_r was small (So et al., 2000, 2001). It should be noted that in the present study the mass ratio of the circular cylinder was 28 times higher than that of the airfoil. In addition, as illustrated in Fig. 7, it can be observed that the fluctuating displacements of the airfoil at all S/D investigated were generally three orders of magnitude higher than those of the cylinder. Therefore, the flow-induced vibration of the cylinder was insignificant. This choice was built into the experimental design so that only the dynamic response of the airfoil was highlighted.

2.3. Vibration measurements

A Polytec Series 3000 Dual Beam Laser Vibrometer was used to measure the bending displacements of the cylinder and the airfoil at their mid-spans in the y-direction. Two optical heads, which were linked through optical fibers to the laser vibrometer, emitted laser beams and received back-scattered signals from the measured vibrating structures. One laser beam was used to record the y-displacement signal, $Y_c(t)$, at the mid-span of the cylinder (or airfoil $Y_a(t)$). Simultaneously, another laser beam was used to monitor the wind tunnel vibration at the same cross-section. The difference of the two signals yielded a displacement measurement with much less contamination from wind tunnel vibration. In addition, the two optical heads were mounted on a rigid structure completely isolated from the wind tunnel. Therefore, it ensured that wind tunnel vibration would not be transferred to the optical heads to affect the accuracy of the vibration measurements.

Torsion (pitching) displacement of the airfoil was measured by pointing the two laser beams at two different locations along the chord at mid-span, one at the shear center and another at 2% chord length from the leading edge. The torsion displacement θ was estimated from the difference of these two signals.

2.4. Measurement of the wake flow

Two hot-wires were employed to measure unsteady velocity fluctuations behind the cylinder and the airfoil. Referring to Fig. 1, one of the hot wires, A, was fixed at $0.4D$ above the upper surface of the airfoil and was used to measure the vortical disturbance carried by the wake to the airfoil. Another hot-wire, B, was fixed at $3D$ downstream of the airfoil trailing edge and $D/2$ offset above the x-axis so as to ensure that the hot wire measured the wake of the cylinder–airfoil system in the post-vortex formation regime. The positions of the hot wires relative to the origin of the coordinate system were varied in the x-direction with changing S/D; however, their y positions were always fixed relative to the airfoil. Thus arranged, the overall wake frequency f_s^* behind the combined cylinder–airfoil system and the wake passing frequency f_s experienced by the downstream airfoil could be deduced from the spectral analysis of the velocity signals.

A particle image velocimetry (PIV) technique (Dantec PIV2000) was used to measure the flow structure and velocity vector of the flow around the coupled cylinder–airfoil system. Seeding the flow with paraffin oil particles of 1 μm diameter, the flow at the mid-section of the structures was illuminated with a scanning laser sheet generated by two 10 W NewWave Research pulsed Argon-ion laser sources, each having a maximum energy output of 120 mJ, and only the green wavelength (532 nm) was filtered for illumination. Digital particle images, each covering 225 mm × 180 mm of the flow field, with identical streamwise and transverse magnifications of 0.09 mm/pixel, were captured using a HiSense Type 13 CCD camera (gain × 4, double frames, 1280 × 1024 pixels). The camera data was transferred to a Pentium III 600 MHz PC with a high-resolution monitor of the same order of pixel density, 256 MB RAM and a 10 GB hard disk. The synchronization between image-capture and illumination was controlled by a Dantec FlowMap Processor

(PIV2100 Type). Each laser pulse lasted for 0.01 μs and the interval between two successive pulses was typically 50 μs, providing a resolution of 0.05 mm particle displacement (~0.56 pixels or 0.003D) per unit flow velocity. Image analysis was carried out with Dantec FlowManager 3D-PIV software. Interrogation windows of 32 × 32 pixels (~0.2D) with 50% overlap in both x- and y-directions were used and only 79 × 63 vectors were sufficient to accurately resolve the in-plane velocity field. The masking function of FlowMap Processor was invoked to minimize the velocity calculation errors created by the image of the vibrating structures. The spanwise vorticity component was then estimated with a spatial resolution of 1.43 mm (~0.0477D). The velocity and vorticity measurement uncertainty were conservatively estimated at 7%, respectively.

When the airfoil was in the post-vortex formation regime of the cylinder wake, the PIV results were used to analyze the oncoming wake excitation characteristics as experienced by the airfoil. As the airfoil moved into the pre-vortex formation regime, the characteristics of the flow propagated downstream of the airfoil was the focus of the PIV study. At different values of S/D, such major characteristics of the modified wake flow as the transverse spacing sv and streamwise spacing d of the KVS vortices residing in the wake were readily obtained by extracting the velocity vector from the PIV data. The characteristics of the modified wake flow thus obtained could help explain the physics of flow-induced vibration of the coupled cylinder–airfoil interaction.

In the present study, the velocity signals of the flow field measured by the hot wire anemometers, as well as the vibration signals $Y_a(t)$ and $\theta_a(t)$ of the airfoil, were sampled with a frequency of 2 kHz per channel, amplified and digitized with a 12 bit A/D board and then recorded in a personal computer. The total sampling time for each record was set at 30 s whereas the spectral resolution was set at $\Delta f = 0.05$ Hz.Such frequency resolutions were sufficient to capture with confidence the variation of the natural frequencies of the interacting cylinder and airfoil, and f_s of the cylinder. The uncertainty of the flow and vibration measurements was estimated to be $\pm 1\%$ and $\pm 3\%$, respectively.

3. Results and discussion

The parameters of importance in the flow-induced vibration problem of a cylinder in a uniform cross-flow are Re, U_r, M^*, and ξ_s, where $U_r = U_\infty / f_c D$ is the reduced velocity, f_c is the natural frequency of the cylinder, $M^* = m_c/\rho_{\text{air}} D^2 b$, and ξ_s denotes the structural damping ratio of the cylinder (So et al., 2000). For the problem of a cylinder and an airfoil in tandem, another important parameter is the gap size S/D between the cylinder base and the leading edge of the airfoil. Furthermore, as S/D and Re vary, the characteristic parameters associated with the KVS, such as f_s, sv and d, are also of importance. However, these parameters are implicit in the variations of S/D and Re and cannot be explicitly specified. Also, Re and U_r are related once the cylinder diameter is fixed. Therefore, f_s cannot be specified a priori. The mass ratios of the cylinder and the airfoil, and their structural damping ratios, are given and fixed for a given experiment. Therefore, among the various parameters, only Re and S/D can be varied. Since the variation of Re was limited by the capacity of the wind tunnel, the only parameter that could be examined in detail was S/D, which was varied from 0.16 to 8.67 in the experiment.

3.1. Two-dimensional justification of the experiments

In most of the experimental and numerical studies mentioned above, two-dimensional (2-D) flow and the associated unsteady forces was tacitly assumed. In order to provide an equal basis for comparison with previous results, a 2-D flow and unsteady force distribution along a finite portion of the cylinder span needs to be established. This means that the measured amplitudes of the bending (plunging) and torsional (pitching) vibrations of the airfoil under KVS-type excitation are tacitly assumed to be 2-D along this finite span and the measurements could be used to validate the BEM discussed in the appendix.

The first point to examine was the 2-D nature of the oncoming flow and the vortex-induced vibration of the elastic airfoil by the KVS. The airfoil was rigidly mounted at its ends. The 2-D nature of the mean flow has been established in Lau (2003). As for the vortex-induced forces, f_s at Re = 10 000 was estimated to be 36.5 Hz, whereas the first mode bending natural frequency of the airfoil $(f_Y)_a$ in still air was 45.4 Hz (Table 1). The two frequencies were so close that the aerodynamic forces induced by the KVS on the airfoil could excite only $(f_Y)_a$. This fact is clearly illustrated in the spectral plots of bending and torsion amplitudes of the airfoil to be presented later. These plots show that only the first mode of vibration was excited for all S/D investigated. It should be noted that for 2-D BEM or finite element modelling (FEM), the structural dynamics of the elastic structures is, in general, assumed to be modelled by a spring-damper-mass system (or 2-dof), which is representative of the location of the maximum amplitude of the first mode vibration at the mid-section of a long structure mounted with fixed ends (So et al., 1999, 2001). Therefore, the present measurements could be used to validate the BEM.

A second point to consider was the 2-D nature of the unsteady aerodynamic forces induced by the KVS along the span of the airfoil. In relation to this, the effect of blockage was first examined. The circular cylinder and the airfoil have created a blockage of 5% and 0.6%, respectively, in the test-section. In terms of the overall flow around the cylinder–airfoil system, the blockage is essentially 5% because the cylinder is upstream of the airfoil. This blockage was not high enough to have a significant effect on the separation characteristics of the cylinder, on the behavior of St (Baban and So, 1991), and on the vortex-induced forces (Norberg, 2003) at the subcritical Re investigated.

Besides blockage, the 3-D nature of the cylinder wake could seriously affect the spanwise distribution of the vortex-induced unsteady forces. In the present experiment, both the circular cylinder and the airfoil were chosen to have a large aspect ratio of 20. It is well known that, in general, the wake flow behind a cylinder is 3-D in nature and the vortex-induced unsteady forces acting on the cylinder are correlated within a finite portion of the span around its mid-plane (Blake, 1986). End plates were often installed on the cylinder to enhance the 2-D nature of the time-averaged pressure fluctuation and the unsteady lift and drag force. The measured spanwise length where the lift force remains correlated depends on the method used to perform the measurements. If the piezoelectric force cell method were used, the measured lift force was found to remain correlate along a greater spanwise length of the cylinder ($>10D$) and the unsteady lift could be assumed to be 2-D over this portion of the cylinder central span (Norberg, 2001, 2003). Therefore, if the cylinder–airfoil system has a sufficiently large aspect ratio in the experiments, and the vortex-induced fluctuating forces and the corresponding vibrations are evaluated in the manner suggested by Norberg (2001, 2003), they could be considered as approximately 2-D along a substantial portion of the central span. It is in this sense that the present measurements of the vibration amplitudes are considered to be approximately 2-D.

A third point to note is that the measurements of the airfoil were obtained in the mid-plane. Even if the wake is 3-D, the effect due to vortex interaction along the span of the cylinder on the shedding behavior at the mid-plane is likely to be minimal (Norberg, 2003). Consequently, the KVS shed from the mid-plane of the cylinder which was responsible for the external excitation of the airfoil would not be much affected by 3-D wake effects. Thus, the conditions created by the experimental setup were as close as can be to those assumed in the BEM; namely that the excitation of the mid-plane of the airfoil was examined under the assumption of a 2-dof model for the structural dynamic response of the airfoil.

3.2. *Wake structure in the absence of the airfoil*

The KVS vortices move past the slender structure and their passage acts as external excitation for the aerodynamic fluctuations of the structure and its associated vibration if it is elastic. In the present study, although the cylinder appears to have a very high stiffness (Table 1), it is elastic to a certain extent. Therefore, it is important to examine whether the vortex-induced vibration would affect the shedding process of the KVS vortices and their subsequent development in the wake. In the absence of an airfoil, the mid-plane evolution of the flow structure was determined from PIV measurements at $\mathrm{Re}=10\,000$. A separate 2-D computation using the FEM code of So et al. (2001) plus a 2-dof model for the structural dynamics was also carried out for comparison. Using a mesh remapping technique, the numerical code was found to be capable of accurately simulating the free vibration of a long slender cylinder with fixed ends in a cross-flow and of resolving the essential features of the fluid–structure interaction. The 2-dof model yields results that are representative of the structural dynamics at cylinder mid-span where the vibration amplitude is largest. The computation was also carried out with $\mathrm{Re}=10000$. Turbulent effects were properly resolved by invoking a k–ε model for the wake flow, while assuming the boundary-layer flow over the cylinder to be laminar. Finally, the relevant parameters for the 2-dof model were derived from the structural properties listed in Table 1.

The measured and computed flow structures in the wake of a circular cylinder are illustrated in Fig. 3. No discernible difference is observed in the vorticity distribution, in the sv and d spacing of the vortices and in the overall wake dimensions (cf. Figs. 3a and 3b). Furthermore, the flow structure in both figures is essentially identical to that given in van Dyke (1982) for a 2-D wake structure at $\mathrm{Re}=10\,000$ (not shown in Fig. 3). The high degree of similarity between the measured and computed wake structure behind the elastic cylinder and the visualized wake structure (van Dyke, 1982) of a rigid cylinder provides strong evidence that the vortex-induced vibration of the cylinder did not have a significant effect on the vortex shedding process in the wake. Hence, the excitation generated from the elastic but highly stiff cylinder can be considered to be the same as that generated from a rigid one. This fact is consistent with the claim by Chen (1987) that if the ratio of cylinder vibration amplitude to its diameter, Y_c/D, is less than 10%, the cylinder vibration has negligible effect on the vortex shedding process. In the present experiment, Y_c/D is about 0.00165%. The high degree of similarity between the measured wake structure and the visualized wake shown in van Dyke (1982) provides additional support for the assumption of 2-D flow and 2-D vortex-induced force in the mid-plane of the cylinder–airfoil system in the present experiment.

Consistent with the investigations of Roshko (1955) and Unal and Rockwell (1988), the pre- and post-vortex formation regimes can also be identified from the present experiment. The boundary between the two regimes is found

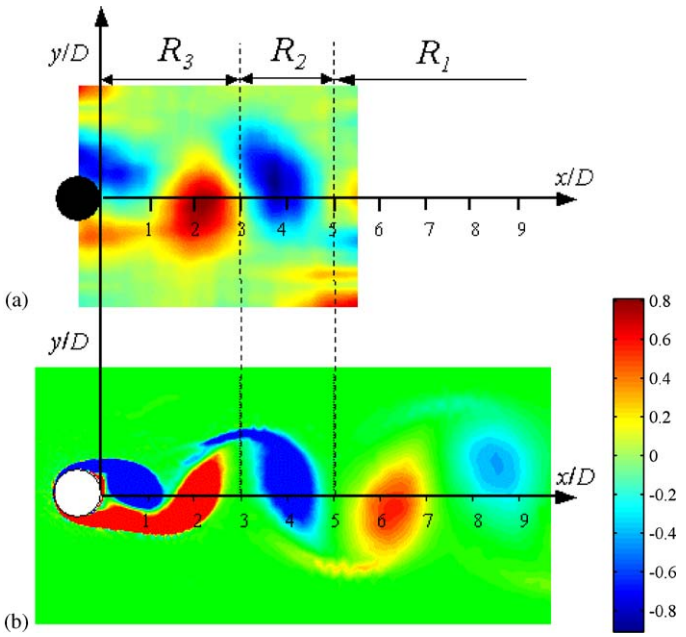

Fig. 3. Nondimensional wake flow structure behind an elastic cylinder with structural properties as listed in Table 1; the vorticity is normalized with respect to U_∞ and D: (a) PIV measurements; (b) FEM calculations (So et al., 2001).

to be located at $S/D=3$ using the ideas of Lee and Kim (1997), and Obara and Matsudaira (1998). In order to facilitate the discussion of the physics of fluid–structure interaction at various S/D in the next few sections, the post-vortex formation regime is further divided into two parts. They are the primary-vortex formation regime, R_2, spanning the range, $3<S/D<5$, and the fully developed-vortex regime, R_1, which extends beyond $S/D=5$. KVS vortices are formed and arranged in two parallel rows in the R_1 and R_2 regime. They become fully developed in the fully developed-vortex regime and move away from the cylinder while convecting downstream. The pre-vortex formation regime is denoted as R_3 in the present study.

3.3. Wake evolution at various gap sizes

A series of wake patterns of the coupled cylinder–airfoil system at different S/D was obtained from PIV measurements. Representative vorticity distributions are plotted in Fig. 4 in order to illustrate how the presence of the airfoil affects the structure of the wake flow behind the cylinder. At $S/D=6$ and 7.33, the airfoil was residing in the R_1 regime. As S/D decreases to 3.33 and 5, the airfoil was moved to the R_2 regime. Further reduction of S/D to 0.33 and 3 brought the airfoil to the R_3 regime. The figures clearly show that the evolution of the overall wake flow was significantly modified dependent on the position of the airfoil. Different wake flow structure would induce different aerodynamic forces on the elastic airfoil, which would lead to different structural response. Therefore, an investigation of the wake modification could provide information on the physics of vortex-induced vibration resulting from a coupled cylinder–airfoil system.

When the airfoil was in the R_1 and R_2 regime, the vortices shed from the upstream cylinder were well organized and formed a KVS pattern (Fig. 4). The evolution of the wake did not appear to be affected by the presence of the slender airfoil. Therefore, as the vortices alternately passed the upper and lower surfaces of the airfoil, they would cause periodic variations of the aerodynamic forces acting on the airfoil. It was this periodic KVS-generated aerodynamic force that gave rise to the strong response of the airfoil in the R_1 and R_2 regime.

As the airfoil moved to the R_3 regime, the external excitation of the airfoil response seemed to have changed. It can be observed that the shear layers emanating from the cylinder was significantly extended downstream due to the presence of the airfoil (Fig. 4). The extended shear layers started to merge at a position $2D$ downstream of the airfoil trailing edge and rolled up to form vortices, which were then shed behind the combined cylinder-airfoil system. Consequently, the airfoil was completely enclosed by the cylinder shear layers. When this happens, the unsteady aerodynamic forces responsible for the airfoil response mainly came from two sources. One was the flow unsteadiness inherent in the shear

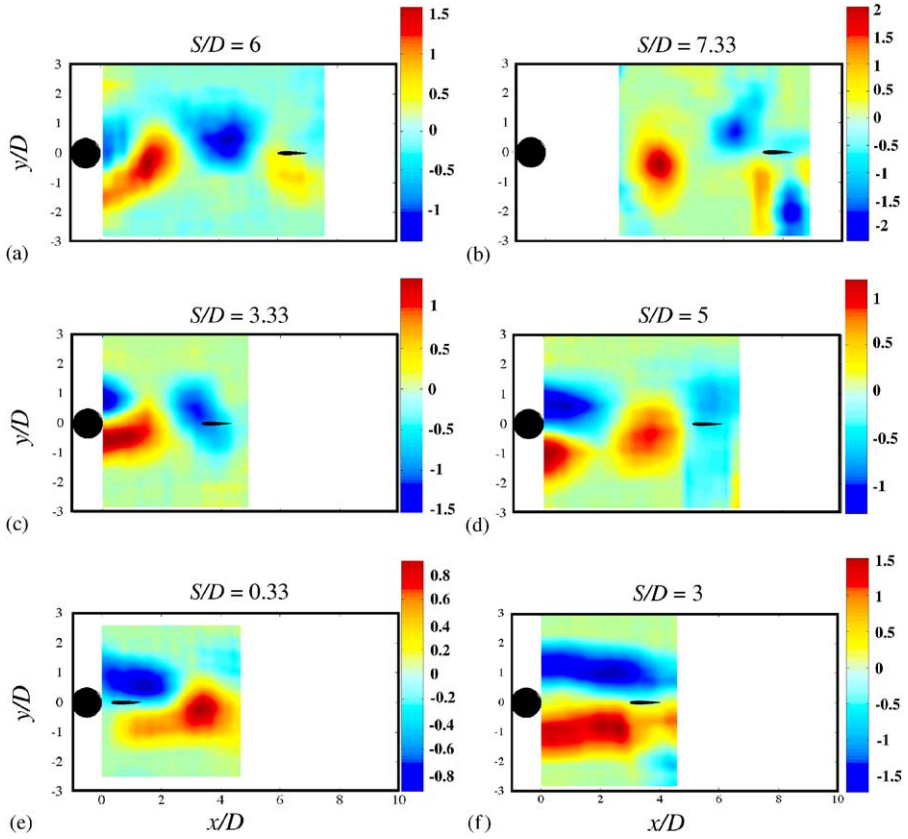

Fig. 4. Nondimensional vorticity distributions of the wake flow structure at various S/D.

layers developing from the cylinder. Another was partial contribution from vortex shedding behind the combined system. Comparing the fluctuating velocity spectra measured by hot-wire A and B, it is clear that only 19% to 32% of the unsteady energy derived from vortex shedding behind the airfoil was responsible for the excitation of the airfoil (Fig. 5).

An important parameter for the vortex-induced vibration of the airfoil is the normalized transverse spacing, sv/D, seen by the airfoil. Here, sv is defined as the transverse distance between the vortex centers above and below the airfoil as captured by the PIV measurements (Fig. 4). This parameter is important because the Biot–Savart law requires the induced velocities and their fluctuations to vary inversely with the third power of the distance (Pozrikidis, 1997). The pressure coefficients of the airfoil will vary with the strength of the induced velocities according to the Bernoulli equation. As the vortices moved closer to the airfoil, the vortex-induced unsteady forces experienced by the airfoil will become stronger.

The variation of sv/D with S/D is shown in Fig. 6. When the leading edge of the airfoil was in the R_1 regime, sv/D was approximately constant at 0.95. This value was determined from the PIV measurements shown in Fig. 4 and was found to be rather similar to that deduced from similar measurements of a single cylinder wake (Fig. 3). The difference between this value and that determined from the KVS theory (Chen, 1972), which was $sv/D = 1.1$ and shown as a constant line in Fig. 6, was about 13.6%. This shows that the theory overestimates the sv/D for both a single cylinder and the case of a cylinder with an airfoil in tandem. The KVS theory does not apply in the R_2 regime as can be seen from the plot in Fig. 6 where sv/D in this regime is substantially lower than that determined from the KVS theory. The constant sv/D in the R_1 regime indicates that the strength of the KVS-excitation on the airfoil depended only on Γ of the approaching vortices and thus on Re (Chen, 1972). Therefore, the evolution of the cylinder wake was significantly modified by the airfoil only if its leading edge is within the R_2 regime.

The overall Strouhal number, $\mathrm{St}^* = f_s^* D/U_\infty$, of the cylinder-airfoil system was determined from the velocity signals of hot-wire B and its variations with S/D are illustrated in Fig. 7. Here, f_s^* is the shedding frequency of the cylinder–airfoil system, while f_s is still used to denote the shedding frequency of a single cylinder in a cross-flow. As the

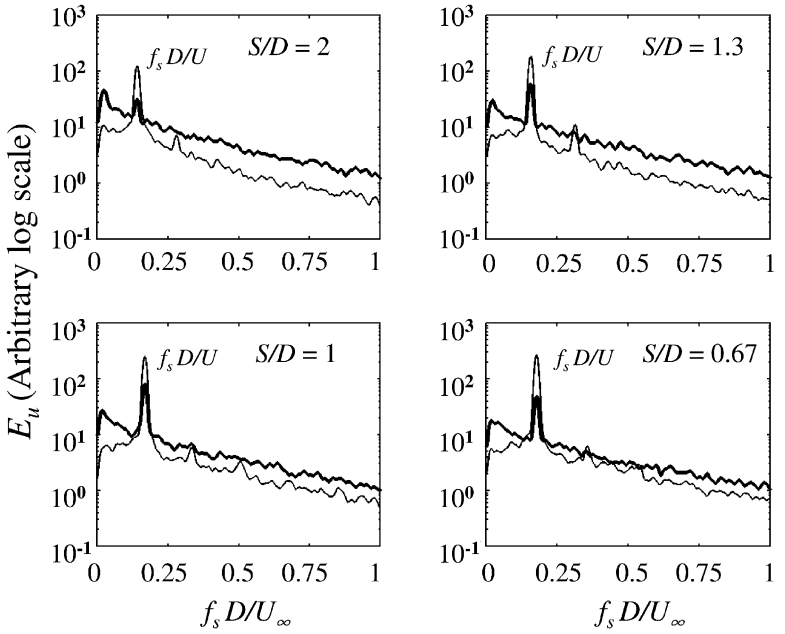

Fig. 5. Power spectra of velocity fluctuations in R_3: ———, hot-wire A; ———, hot-wire B.

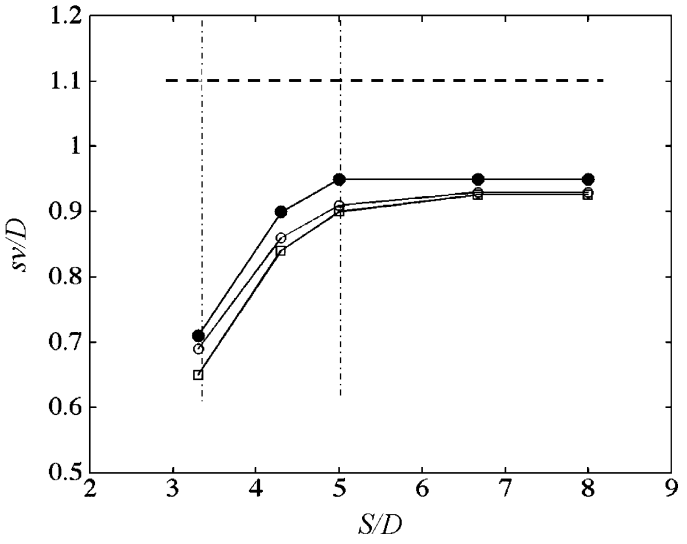

Fig. 6. Variations of transverse spacing of KVS rows with S/D: ●, PIV measurements of elastic circular cylinder; ○, FEM calculations of elastic circular cylinder; □, van Dyke flow visualization of a rigid circular cylinder in a cross-flow, – – – –, Chen's (1972) KVS theory; dot-dashed lines indicate the boundaries of R_1, R_2 and R_3.

airfoil moved from far downstream towards the cylinder, such that its leading edge is within the R_1 and R_2 regime, St remains fairly constant at 0.194. This represents a 4.4% deviation from the measured St = 0.203 of the same cylinder without airfoil and a 3% deviation from a single rigid cylinder at the same Re (Zdravkovich, 1997). The result lends support to the fact that, in this range of S/D, the airfoil did not have a significant effect on f_s and the evolution of the wake behind the cylinder–airfoil system resembles that of a single cylinder. However, when the leading edge is within the boundary between R_2 and R_3 ($3 < S/D < 3.3$), St is greatly modified. There is a drastic drop in St from $S/D = 3.33$

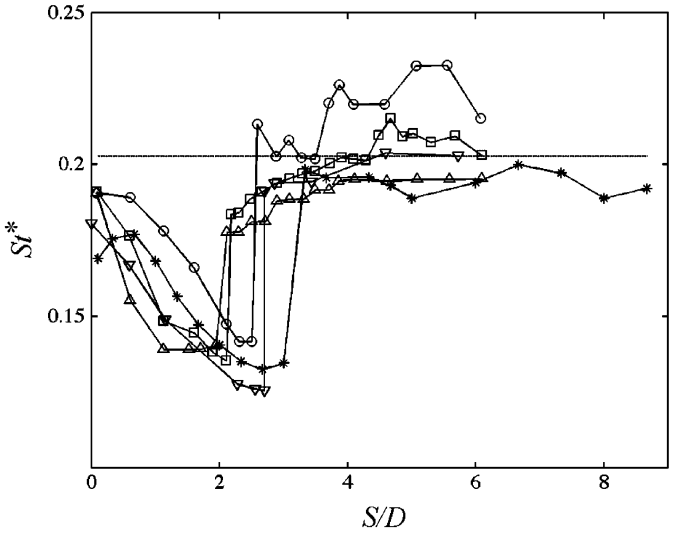

Fig. 7. Variations of overall Strouhal number St* with S/D: —*—, elastic cylinder/airfoil system in the present study; · · · · · · ·, elastic cylinder only in present study. Rigid cases: —○—, Re = 6700 (Ozono, 1999); —□—, Re = 17 000 (Ozono, 1999); —Δ—, Re = 25 000 (Ozono, 1999); —▽—, Roshko (1955).

to 3. Such a drastic drop reflects the fact that there is a transitional change in the flow character around the airfoil (Figs. 4(c) and (f)). At $S/D = 3.33$, alternating KVS vortices, already formed from shear layer roll-up, still approach and pass over the airfoil. Therefore, hot-wire B detects a rather strong periodic vortex passage signal. When S/D was reduced to 3, the airfoil appeared to be embedded in the lengthened shear layers emanating from the cylinder. As a result, alternating KVS vortices form at locations downstream of the airfoil trailing edge. No periodic signal could be detected by hot-wire A, leading to a minimum at $S/D \approx 3$. As the leading edge of the airfoil moved further upstream into R_3, the vortex formation length was reduced and the KVS vortices continued to form behind the combined structure (clearly visible in Fig. 4). Since the vortex shedding frequency is inversely proportional to the vortex formation length (Unal and Rockwell, 1988), a reduction in S/D would give rise to an increase in St.

It is worthwhile to note that the variation of St with S/D shares a similar trend with those reported in Roshko (1955) and Ozono (1999), with both investigations involving a rigid cylinder-plate combination (Fig. 7). Ozono (1999) examined the variation of St with S/D with a setup where the plate chord length was the same as the cylinder diameter, in a Re range of 6700 to 25 000. Flow-induced vibration effect was not considered. He found that the variation of St versus S/D depended on Re. The dependence was reflected in a shift of the critical S/D where the minimum St occurred. The critical S/D reduced from 3 to 2 as Re was increased from 6700 to 25000. From these results (Fig. 7), it can be deduced that the fundamental physics of wake evolution is rather similar for the few cases examined, including the present setup where the cylinder–airfoil system is elastic.

3.4. Vibration responses of the structures

The variations of the root mean square (rms) value of the bending displacements of the cylinder and the airfoil, $(Y_c/D)_{\mathrm{rms}}$ and $(Y_a/D)_{\mathrm{rms}}$, respectively, and the torsion displacement $(\theta_a)_{\mathrm{rms}}$ of the airfoil with S/D are plotted in Fig. 8. The behavior in each of the regimes is examined separately.

R_1 regime ($5 < S/D \leqslant 8.67$): Since St changes slightly with S/D in this regime, the KVS excitation experienced by the airfoil also changes slightly and the values $(Y_c/D)_{\mathrm{rms}}$, $(Y_a/D)_{\mathrm{rms}}$ and $(\theta_a)_{\mathrm{rms}}$ are fairly constant. So et al. (1999) found that when an elastic airfoil/blade is exposed to an oncoming KVS disturbance, the levels of the plunging and the pitching vibration of the airfoil/blade are mainly determined by c/d of the KVS alternating vortices. Therefore, the values of $(Y_a/D)_{\mathrm{rms}}$ and $(\theta_a)_{\mathrm{rms}}$ only show mild variations around 2.5×10^{-3} and 1.5×10^{-5}, respectively, with S/D. Plunging of the cylinder Y_c is excited by the self-generated aerodynamic forces arising from the vortex shedding processes. The self-excitation was insensitive to the airfoil position in the present experiment. Therefore, the measured $(Y_c/D)_{\mathrm{rms}}$ value was fairly constant at around 7.5×10^{-6}. It should be noted that $(Y_c/D)_{\mathrm{rms}}$ is less than $(Y_a/D)_{\mathrm{rms}}$ by

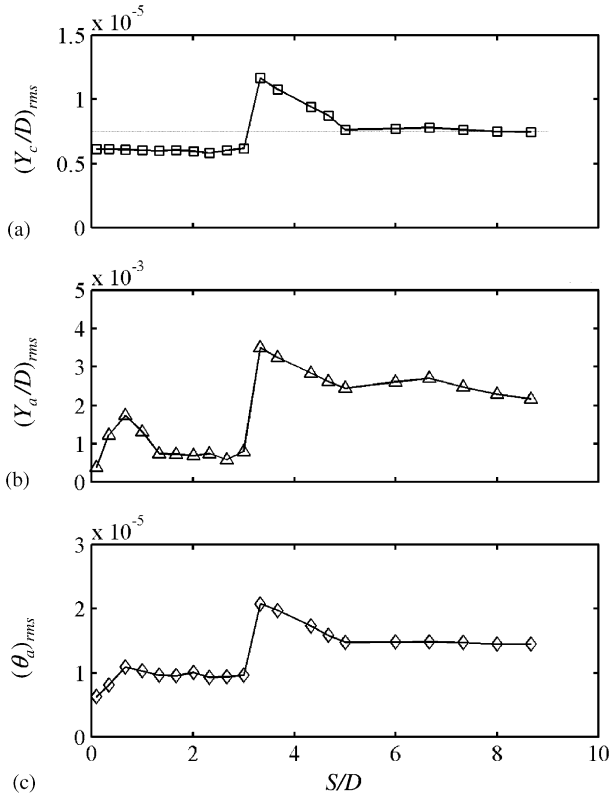

Fig. 8. Variations of the r.m.s. vibration amplitude with S/D: (a) cylinder bending; (b) airfoil bending; (c) airfoil torsion.

more than two orders of magnitude, providing firm evidence for neglecting cylinder vibration effects on its vortex shedding for the present setup.

R_2 regime ($3.3 \leqslant S/D \leqslant 5$): The structural responses, $(Y_c/D)_{\mathrm{rms}}$, $(Y_a/D)_{\mathrm{rms}}$ and $(\theta_a)_{\mathrm{rms}}$, share the same trend in this regime (Fig. 8). The r.m.s. vibration amplitudes increase from $S/D=5$, reach a maximum at $S/D=3.1$, and then drop sharply to a minimum at $S/D=3$.

As pointed out earlier, sv/D of the oncoming alternating KVS vortices experienced by the airfoil decreases as the airfoil moved closer to the base of the cylinder. Usually a KVS with smaller sv/D induces higher mean velocity and gives rise to higher fluctuations in the flow field around the airfoil as a consequence of the Biot–Savart law (Pozrikidis, 1997). It implies that, for smaller gap size, the oncoming vortices would create faster transverse flow around the airfoil. This behavior is supported by laser Doppler anemometer (LDA) measurements at the airfoil leading edge (Fig. 9(a)). The amplitude of the mean transverse velocity v_{mean} at $S/D=3.3$ is approximately 2.9 times those at $S/D=4.3$ and 5, but the corresponding velocity fluctuations do not show any significant differences. The increase in v_{mean} also implies that the strength of the KVS vortices approaching the airfoil is reduced with S/D in R_2. This is readily observed from the variation of circulation Γ of the oncoming vortices with S/D in Fig. 9(b). The circulation is calculated by integrating along a contour enclosing a piece of oncoming vorticity patch obtained from PIV measurements (Fig. 4). Higher v_{mean} and Γ would induce higher aerodynamic lift on the airfoil. This observation is consistent with the study of Streitlien et al. (1996). They found that in the case where a vortex street is interacting with a blade, the aerodynamic lift of the blade is proportional to the strength of the induced transverse velocity produced by the vortex street. Therefore, the magnitude of $(Y_a/D)_{\mathrm{rms}}$ and $(\theta_a)_{\mathrm{rms}}$ increase with decreasing S/D due to a progressive increase in the aerodynamic lift of the airfoil.

The increasing strength of the KVS vortices with decreasing S/D is also responsible for the similar trend for the magnitude of $(Y_c/D)_{\mathrm{rms}}$, as shown in Fig. 9(a), although it is in general two orders of magnitude weaker than the airfoil vibration. Formation of strong KVS vortices from the vibrating cylinder appears to create stronger suction base pressure behind the cylinder, which induces stronger unsteady forces on the cylinder and results in higher vibration response. This is in contrast with previous experiments with a rigid circular cylinder (Roshko, 1955) ora rigid

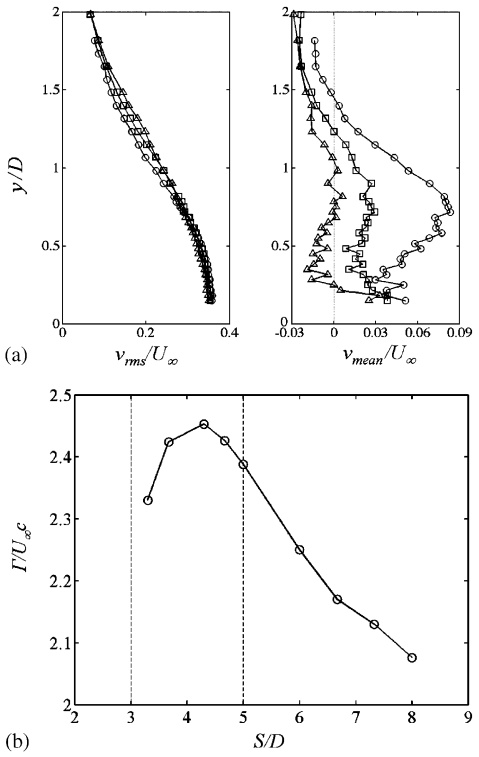

Fig. 9. (a) LDA transverse flow velocity measurements at the airfoil leading edge: ○, $S/D=3.3$; □, $S/D=4.3$; Δ, $S/D=5$. (b) Variations of the circulation of KVS vortices approaching the airfoil with S/D; dashed lines indicate the boundaries between R_1, R_2 and R_3.

rectangular cylinder (Mansingh and Oosthuizen, 1990) in tandem with a rigid splitter plate. Both experiments revealed that, beyond the pre-vortex formation regime R_3, the suction pressure behind the upstream cylinder is fairly constant at a value weaker than the case without the splitter plate. In fact, similar substantial enhancement of vibration magnitude of an elastic cylinder in the presence of a downstream bluff body was previously reported in Zdravkovich (1985) and Lakshmana Gowda and Prabhu (1987).

R_3 regime ($0.167 \leqslant S/D \leqslant 3$): When the leading edge of the airfoil was moved to $S/D=3$, i.e., the boundary of R_3, the airfoil caused a sudden extension of the vortex formation length and was embedded by the two shear layers emanating from both sides of the cylinder. In this situation, the cylinder was no longer excited by the alternating passing KVS vortices but by the inherently weak oscillations of the unstable shear layers. Roshko (1955) observed this phenomenon in his experiments and that, at a similar critical S/D, the base pressure of the cylinder would increase sharply. As the base pressure increases, the two shear layers would move away from each other, thus forcing them to extend further downstream. Since the pressure in the region just downstream of the combined structure is relatively lower than that behind the cylinder, the pressure difference prompts the two shear layers to merge downstream of the combined structure. Consequently, the separation between the two shear layers becomes very small, and the two shear layers tend to roll up to form vortices with a much weaker Γ. The resultant weaker aerodynamic forces on the airfoil due to weaker excitation vortices just downstream of airfoil explains the sharp drop in the magnitudes of $(Y_c/D)_{\rm rms}$ $(Y_a/D)_{\rm rms}$ and $(\theta_a)_{\rm rms}$ as the airfoil moved across the boundary of the R_2 regime into the R_3 regime (Fig. 8).

The structural response of the cylinder $(Y_c/D)_{\rm rms}$ did not show any further change in the range, $0.167<S/D<3$, because the major source of oscillating aerodynamic force induced on it is now mainly derived from the weak instability of the separating shear layers. The airfoil responses, $(Y_a/D)_{\rm rms}$ and $(\theta_a)_{\rm rms}$, in general, do not show significant variations in the same S/D range but there are peaks at $S/D\approx0.67$. The peak value of $(Y_a/D)_{\rm rms}$ is almost four times higher than its minimum located at $S/D\approx0.167$, while the ratio of the peak value of $(\theta_a)_{\rm rms}$ to its minimum at $S/D\approx0.167$ is approximately 1.8. The explanation for the occurrence of the peaks is given in the next section.

Generally, the ratio of $(Y_a/D)_{\rm rms}$ to $(Y_c/D)_{\rm rms}$ does not show any significant variation with S/D and stays approximately constant at 300. This high ratio could be attributed to the difference in structural properties of the two structures, and provides further evidence that the cylinder could be considered as rigid in the present setup.

3.5. Spectral behavior of cylinder–airfoil system

The spectra of the bending displacement of the airfoil at all measured S/D are shown in Fig. 10. There are two dominant peaks in the bending displacement spectra. The peaks occurring around 45 Hz correspond to the first mode bending natural frequency $(f_{Y1})_a$ of the airfoil. These values are not exactly equal to the f_Y given in Table 1. In fact, they represent the first mode bending natural frequency of the airfoil in the coupled fluid–airfoil system and the difference could be attributed to the effect of fluid-structure interaction. Since the oncoming St experienced by the airfoil is a function of S/D, the degree of fluid-structure interaction experienced by the airfoil also changes with S/D. As a result, the bending natural frequency of the airfoil in the coupled fluid-structure system is not constant but takes a lower value for all S/D examined (Fig. 11). The $(f_{Y1})_a$ increases mildly in the R_3 and R_2 regime, and remains fairly constant in the R_1 regime. The variation of $(f_{Y1})_a$ is about 10% of the mean value, which is much greater than an error margin of $\pm 3\%$ in the vibrometer measurement; therefore, the variation shown in Fig. 11 is real. Similar shift in natural frequency has also been observed in the studies of So et al. (2000, 2001) and Zhou et al. (2001).

The other dominant peak in the airfoil bending spectra (Fig. 10) represents the flow-induced structural response caused by external excitation deriving from the oncoming KVS vortices. In order to understand this behavior better, the total bending energy $(E_Y)_a$ of the airfoil calculated by integrating the area under the measured bending spectra (Fahy 1985) is plotted in Fig. 12. The components attributed to St and $(f_{Y1})_a$ are also shown in Fig. 12. In the R_2 and R_1 regime, $S/D > 3$, where alternating KVS vortices are found, the total bending energy decreases with increasing S/D. Generally, the contribution of St reduces gradually due to the weakening of the KVS vortices while they are convecting downstream. Its percentage contribution to the total bending energy reduces from 44% at $S/D = 3.3$ (which is equivalent to 56% of the $(f_{Y1})_a$ component) to 29% at $S/D = 8.67$. In the R_3 regime, $S/D < 3$, the major source of excitation is the weak oscillations of the developing shear layers. The resultant energy of bending due to shear-layer-induced vibration is very low, being one order of magnitude lower than that of the vortex-induced vibration in the R_2

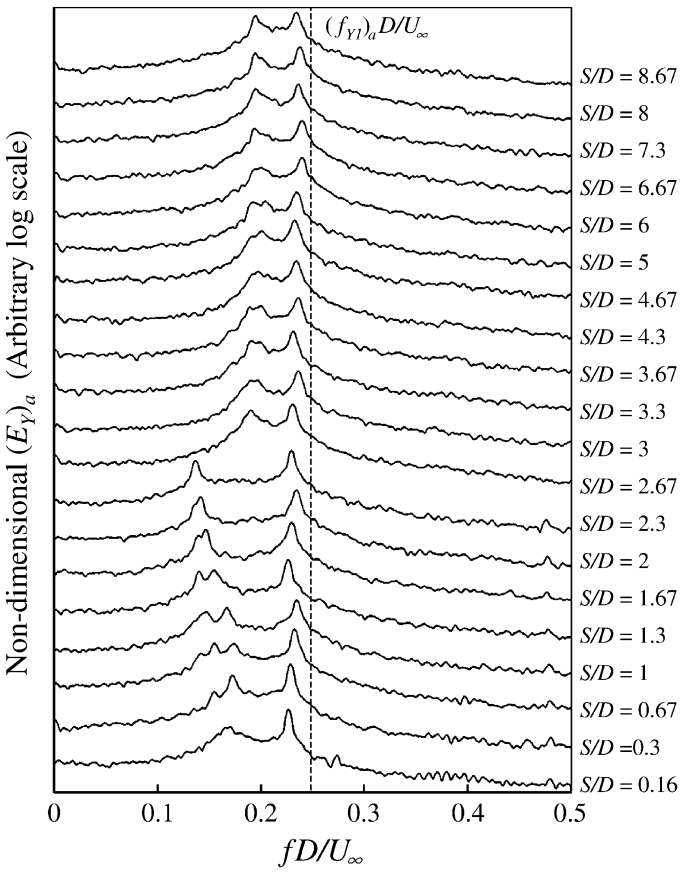

Fig. 10. Energy spectra of airfoil bending vibration.

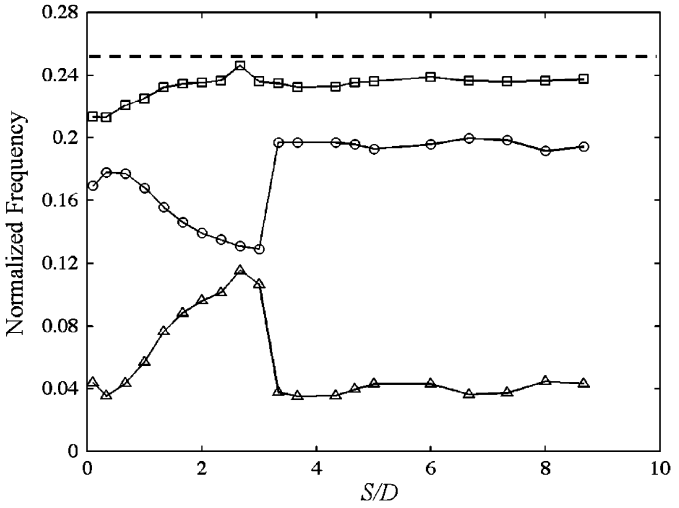

Fig. 11. Variations of the normalized frequencies with S/D: —□—, normalized first mode bending frequency $(f_{YI})_a$ of airfoil in the cylinder/airfoil system; —○—, Strouhal frequency St; —Δ—, difference between the two frequencies; – – – – –, first mode bending frequency of airfoil in still air.

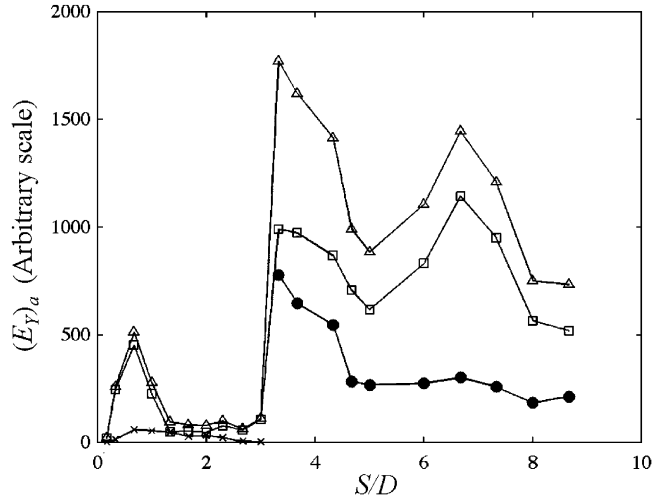

Fig. 12. Variations of the bending vibration energy of the airfoil with S/D: —□—, energy component at first mode bending frequency $(f_{YI})_a$; —×—, energy component at St in pre-vortex formation regime; —●—, energy component at St in post-vortex formation regime; —Δ—, total energy.

and R_1 regime. There is an exception at $S/D = 0.67$, where the bending energy $(E_Y)_a$ is 7.8 times higher than that due to vortex shedding. A careful examination of the variation of the normalized frequency difference between St and $(f_{YI})_a$ in the fluid–airfoil system over the S/D range investigated (Fig. 11) reveals the smallest difference around $S/D = 0.67$. This suggests that, at this gap size, the frequency excitation of vortex shedding might be quite close to the airfoil natural frequency. Consequently, the airfoil response is close to resonance and the airfoil oscillates to absorb high vibration energy. The difference between the two frequencies increases from $S/D = 1$ to 3, making the resonance behavior not possible to occur. From $S/D = 3.3$ onwards, the normalized frequency difference between St and $(f_{YI})_a$ remains fairly constant.

In regime R_1, a notable peak of bending vibration energy of the airfoil occurs at $S/D = 6.67$ (Fig. 12). The occurrence of this peak could be explained by an examination of the variation of the properties of the oncoming KVS vortex street, which are well established in this regime (Fig. 4). The flow-induced excitation created by an oncoming KVS rows is affected by sv, Γ, and the normalized frequency parameter c/d along the same row (So et al., 1999; Luk et al., 2004).

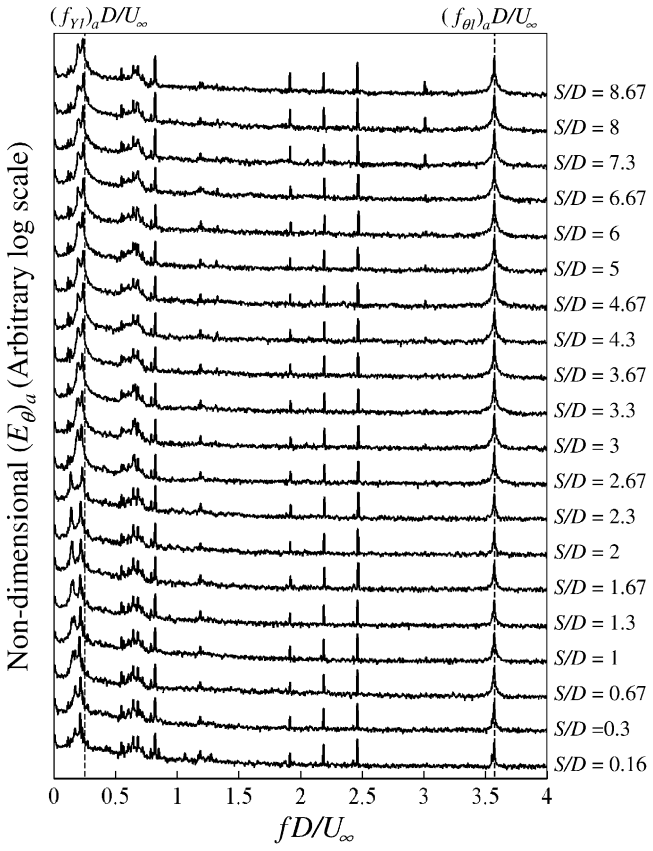

Fig. 13. Energy spectra of airfoil torsional vibration.

In regime R_1, *sv* is a fairly constant (Fig. 6) and is not important. On the other hand, Γ drops steadily with S/D (Fig. 9); this implies that the unsteady forces acting on the airfoil are also decreasing. Therefore, c/d is the only parameter that could give rise to the appearance of the peak at $S/D = 6.67$. According to So et al. (1999), the bending amplitude of an elastic airfoil under KVS excitation increases monotonically with c/d as long as $c/d < 0.5$. Following the procedures outlined in Luk et al. (2004), the estimated c/d at $S/D = 5$, 6.67 and 8 in the present study are 0.191, 0.2 and 0.191, respectively. It appears that c/d is largest at $S/D = 6.67$, therefore, its effect could be responsible for the appearance of the peak vibration energy there.

The flow-induced torsional vibration shows similar characteristics to those of bending (Fig. 13). The same set of St is found in the $(E_\theta)_a$ spectra. The common peak at $f = 652.1$ Hz is the first mode torsional natural frequency of the airfoil, $(f_{\theta 1})_a$, in the coupled fluid–airfoil system. Note the slight shift of torsional frequency from 652.9 Hz in still air to 652.1 Hz as a result of fluid–structure interaction. Furthermore, a distinct third peak can be identified at $f \approx 45$ Hz, which is the natural bending frequency of the fluid–airfoil system. This is a clear indication that there is a strong coupling between the bending and torsional modes of vibration of the airfoil.

4. Coupled resonance of downstream structure

A number of experimental and numerical studies have attempted to show that the aerodynamics of a circular cylinder in a cross-flow can be altered by simply placing a splitter plate in the cylinder wake. When the plate is in the R_3 regime, the levels of the fluctuating aerodynamic forces and the vibrations of the cylinder are stabilized by the introduction of a splitter plate. This conclusion was drawn because, in these studies, the effect of the aero-elastic behavior of the splitter plate was neglected; hence, subsequent flow-induced vibration under the excitation of the modified wake flow was not considered.

The observed vibration of the elastic airfoil at $S/D=0.67$ shows that the above conclusion has to be re-examined. In the R_3 regime, the vortex-induced vibration of the airfoil should be minimal because alternating KVS vortices form behind the entire cylinder–airfoil system. However, the appearance of a peak at $S/D=0.67$ shows that a possible resonance, of the structural type, could occur as f_s of the modified cylinder wake or its higher harmonics approaches $(f_{YI})_a$ of the coupled fluid–airfoil system (Fig. 11). The magnitude of the peak was not as high as the pure vortex-induced vibration in the R_2 regime. It could be conjectured that the weak magnitude was the result of a finite difference between f_s and $(f_{YI})_a$ at this particular S/D (Fig. 11), hence full resonance has yet to occur. Consequently, only a small amount of resonant energy was transmitted to the airfoil (Fig. 5). The PIV vorticity measurements in Fig. 4 reveal that, for $S/D\leqslant 3$, the airfoil is completely embedded between the two developing shear layers extending from the cylinder base and is far away from the well-established KVS vortices developed behind the entire cylinder–airfoil system. Lin et al. (1995) used high-image-density PIV to capture the instantaneous near-wake structure of a circular cylinder at $\mathrm{Re}=10000$. Their captured images clearly showed that the shear layers created small-scale Kelvin–Helmoltz vortical structures shortly after separation from the cylinder and continuously fed the formation of large-scale KVS vortices. The passage of these small but concentrated Kelvin-Helmoltz vortices could contribute to the excitation of the airfoil. However, based on available data, the alternate formation of large-scale vortices downstream could still be the cause of the near structural resonance observed. Regardless of the mechanisms responsible for the occurrence of resonance, the observation shows that whenever coupled fluid–structure interaction is present, such as a bluff body and a slender structure in tandem, the assumption of the downstream structure being rigid is not appropriate, even though its stiffness is 'high'. This is because the downstream structure could resonate with f_s, thus vibrating violently and affecting the coupled fluid-structure system.

To further illustrate this point, a fluid–structure interaction experiment with an elastic cylinder and an elastic thin plate of rectangular cross-section was performed. The structural properties of the cylinder and the plate are listed in Table 2. The stiffness of the two structures was chosen so that they were 'low' enough to exhibit aeroelasticity effects. The free-stream velocity U_∞ was set at 17 m/s, thus giving a $\mathrm{Re}=9000$, slightly less than that of the cylinder-airfoil experiment. The small difference in Re was not significant enough to cause discernible changes in the wake structure and its evolution.

The cylinder was made of a hollow acrylic tube with outer diameter $D=8$ mm.The downstream plate was made of stainless steel, with a rectangular cross-section of length $L=10$ mm and thickness $t=1$ mm.The thickness ratio of the plate, t/D, is 12.5%, which is slightly different from the corresponding value of 12% in the coupled cylinder–airfoil system. Unless otherwise stated, the experimental techniques and procedures used were basically the same as those used in the cylinder–airfoil experiments.

The amplitude of vibration of the acrylic cylinder was measured to be approximately 0.1% of D and according to arguments presented in Section 3.2 a small vibration amplitude does not have any influence on the evolution of the wake structure. The variation of St of the cylinder–plate system is compared with the result of the cylinder–airfoil system, and the experimental investigations reported in Zdravkovich (1997), and Hasan and Budair (1994) (Fig. 14). The work of Zdravkovich (1997) involved two rigid cylinders in tandem, whereas Hasan and Budair (1994) studied the fluid–structure interaction of a rigid rectangular cylinder and a rigid downstream splitter plate. It can be observed that St is a function of Re, and geometry and properties of the structures. For the present experiments, the geometry of the downstream slender structure does not appear to have much effect on the vortex shedding process of the upstream cylinder in the R_2 and R_1 regime. However, there is a substantial difference in St in the R_3 regime. It appears that the

Table 2
Structural properties of the cylinder and the thin plate in a cylinder/plate system

Quantity	Circular cylinder	Thin plate
Dimension (mm)	Outer diameter $D=8$ Inner diameter = 6	Chord length $c=10$ Thickness t = 1
Span b (m)	0.6	0.6
Material	Hollow acrylic	Stainless steel
Mass/unit length (kg/m)	0.02	0.07
Bending stiffness/unit span k_Y ($\mathrm{N/m^2}$)	1315.27	9606.14
Bending natural frequency in still air f_Y (Hz)	41.02 (First mode)	59.57 (First mode)
Mass ratio $M^*=m/\rho_{\mathrm{air}}D^2b$	260.4	911.4
Reduced velocity $U_R=U_\infty/f_YD$	51.8	35.67
Nondimensional bending natural frequency f_YD/U_∞	0.019	0.028

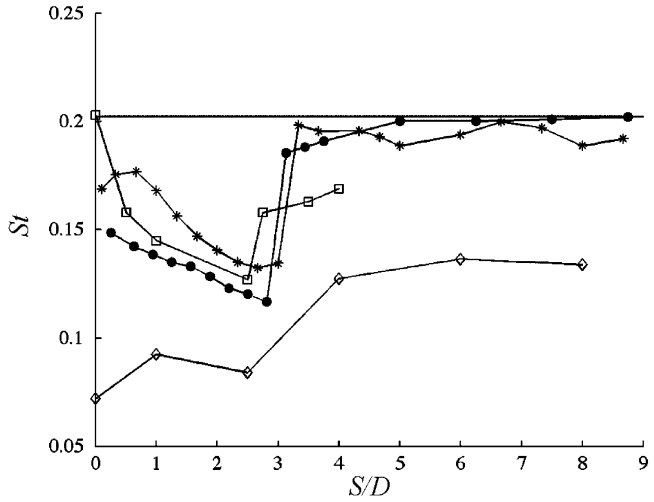

Fig. 14. Comparison of the variations of St with S/D: —●—, elastic cylinder/plate system at Re = 9000; —*—, elastic cylinder/airfoil system at Re = 10 000; ———, elastic cylinder alone at Re = 9000; – – – – –, elastic cylinder alone at Re = 10 000; —□—, rigid circular cylinders in tandem at Re = 8000 (Zdravkovich, 1997); —◇—, rigid rectangular-cylinder/plate system at Re = 16 000 (Hasan and Budair, 1994).

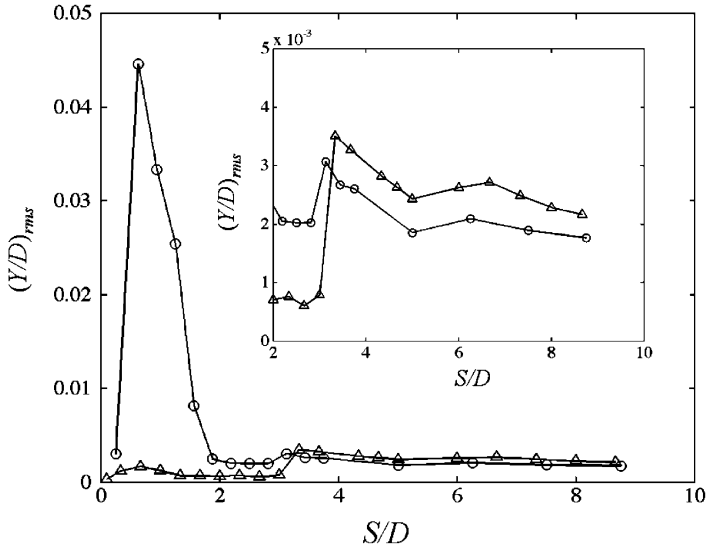

Fig. 15. Comparison of the airfoil and plate structural response: —Δ—, airfoil; —○—, plate. The small figure is a magnified view for $2 \leqslant S/D \leqslant 10$.

shear layer oscillations associated with a thin plate were less unsteady and gave rise to lower frequency vortex shedding in the wake.

The structural response of the elastic plate is compared with that of the airfoil at all gap sizes in Fig. 15. The overall trend for the two structures is similar throughout the whole wake. The difference between the levels of the two curves could be attributed to the different aerodynamic characteristics of the cross-section of the structure. However, an exceptionally high response is found at $S/D = 0.6$ for the cylinder–plate system. Fig. 16 shows the spectrum $(E_Y)_p$ of the plate bending energy at this value of S/D. The first mode bending frequency $(f_{Y1})_p$ was 58.97 Hz, lower than 59.57 Hz measured in still air for the cylinder–plate system (Table 2). It can be seen that the vortex shedding frequency, 302 Hz, was very close to the fifth bending mode frequency, $(f_{Y5})_p = 318$ Hz, of the thin plate. Therefore, it is possible that the thin plate was resonating with this fifth bending mode, effectively absorbing energy from vortex shedding. This could

lead to a resonance behavior at $(f_{YI})_p$ and a high peak in the vibration amplitude (Fig. 15). The plate resonant behavior is nearly a perfect harmonic oscillation, with frequency corresponding to the first mode bending frequency $(f_{YI})_p$ of the coupled fluid–plate system. A phase plot of Y_p/L versus $\dot{Y}_p/U_\infty$ for the plate vibration is illustrated in Fig. 17. The clear loops in the phase plot provide strong evidence for the occurrence of structural resonance and explain the significant contribution of the first bending mode energy (Fig. 16). The phase plot of Y_a/c versus $\dot{Y}_a/c$ for the airfoil vibration at $S/D=0.67$ is also included in Fig. 17 for comparison. It shows that the airfoil in the coupled cylinder–airfoil system had not fully developed into a resonant state. Since the thin plate exhibited structural resonance at a lower S/D than in the airfoil case, it received little excitation energy from the alternating KVS and the resonance was mainly driven by shear-layer-induced vibration.

The occurrence of structural resonance of the thin plate and the high structural response of the airfoil at its first mode bending natural frequency clearly indicate that the assumption of structural rigidity in the study of coupled fluid–structure interaction of two structures in a cross-flow is inappropriate because resonance might occur with higher-order vibration modes.

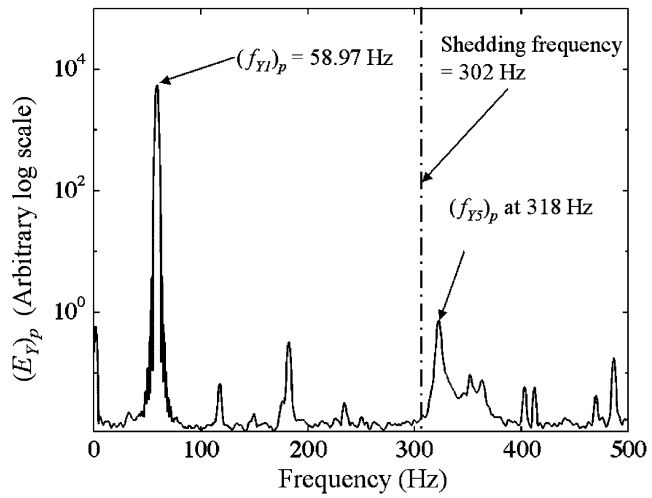

Fig. 16. Bending energy spectrum of an elastic plate at $S/D=0.67$.

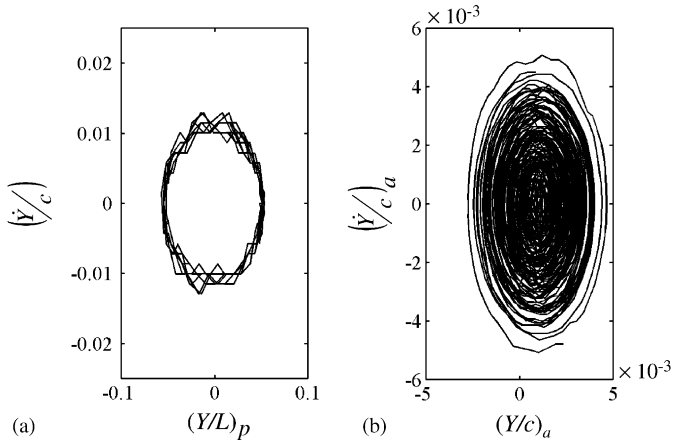

Fig. 17. Phase plots of structural vibration: (a) plate at $S/D=0.6$; (b) airfoil at $S/D=0.67$.

5. Conclusions

Wind tunnel experiments have been carried out to study the wake-induced vibration of an elastic slender structure, a NACA0012 airfoil, placed in tandem with an upstream circular cylinder at Re = 10000. The aspect ratio of both structures was 20 and the fluid–structure interaction problem was considered essentially 2-D. The structures were rigidly mounted at both ends. The wake flow pattern, bending (plunging) and torsional (pitching) vibrations of the blade were measured using PIV, hot-wires, and laser vibrometer, over a range of gap size S measured along the x-axis from the cylinder base to the leading edge of the downstream structure.

Three regimes of wake flow behind the cylinder can be identified: they are the pre-vortex-formation regime R_3 ($0 < S/D < 3$), the primary-vortex formation regime R_2 ($3 < S/D < 5$) and the fully developed-vortex regime R_1 ($S/D > 5$). The flow-induced vibration behavior of the airfoil is different in each of these three regimes.

The structural responses of the cylinder and the airfoil, $(Y_c/D)_{\mathrm{rms}}$, $(Y_a/D)_{\mathrm{rms}}$ and $(\theta_a)_{\mathrm{rms}}$, are not dependent on the variation of S/D in the R_1 regime. However, as the airfoil moved into R_2, the level of the airfoil vibration increases with decreasing S/D due to a narrowing of the transverse spacing of the oncoming KVS vortices. The narrower the transverse spacing of the oncoming vortices, the higher the structural response of the airfoil becomes. The Strouhal number St of the wake in the R_1 and R_2 regime is fairly constant and is close to the value determined for an isolated rigid cylinder in a cross-flow.

A different wake mechanism occurs when the airfoil enters into the R_3 regime. The shear layers on both sides of the cylinder, and the vortex formation length, are extended. The shear layers meet each other downstream of the airfoil and then roll up to form KVS vortices in the wake of the entire cylinder–airfoil system. The airfoil appears to be enclosed by the shear layers. The extension of the vortex formation length results in a sharp drop in St. The airfoil vibration appears to be stabilized in R_3 due to the weak shear layer oscillations and the weak excitations resulting from vortex shedding far downstream. There was an exception at $S/D = 0.67$. At this location, the vortex shedding frequency of the cylinder–airfoil system is close to the first mode bending frequency of the coupled fluid–structure system and resonance might occur. The possibility of resonance occurring is further highlighted by a complementary experiment of an elastic cylinder and an elastic thin plate in tandem. It is found that, in the same R_3 regime, the vortex shedding frequency matched the fifth bending mode frequency of the plate, and resonance does indeed occur. Together, these two experiments show that it is not appropriate to simply assume the structures to be rigid without knowing their structural mode responses in any fluid–structure interaction problem, even though their stiffness might be very 'high'. The structures might resonate, and their vibrations would alter the entire fluid–structure interaction, once their structural natural frequencies match those of the flow-induced forces.

The vibration amplitude measurements of the airfoil response in the R_1 and R_2 regime have been used to validate the BEM numerical model developed by So et al. (1999) to simulate fluid–structure interaction problems where there are oncoming vortices in the form of a KVS pattern. Good agreement between calculations and measurements has been obtained. The good agreement further validates the viability of the BEM numerical model in calculating flow-induced vibration problems involving vortex-street and elastic structures.

Acknowledgements

Funding support given under Grant Nos. PolyU 5128/98E and PolyU 5161/00E by the Research Grants Council of the Government of the HKSAR is gratefully acknowledged.

Appendix: Validation of the numerical vortex–airfoil interaction model

The results of the present coupled interaction of a cylinder and an elastic airfoil can be used to validate numerical model designed for complex vortex–blade interaction problems. Using the time marching technique proposed by Jadic et al. (1998), So et al. (1999) developed a 2-D BEM numerical model capable of fully resolving the coupled aerodynamic and structural response of the fluid–blade interaction created by an upstream vortical flow propagating in a KVS pattern. The numerical model is designed to estimate the flow-induced vibration of multiple blades in turbomachinery cascades under the excitation of oncoming periodic vortical disturbance. In order to establish the credibility of the numerical model, Lau et al. (2002) performed a systematic analysis of the numerical model by simulating a series of vortex–blade interaction problems with increasing complexity, and compared the simulation results with existing experimental data. The simulation of a classical blade-vortex interaction problem, at which a discrete vortex is allowed to pass over a rigid blade, agreed well with experiments and was capable of predicting all the essential blade

aerodynamics. The second simulation was the interaction of an elastic slender structure placed between two rows of oncoming alternating vortices. The results were compared with the elastic cylinder–plate interaction experiment described in Section 4. They used a NACA0010 airfoil to approximate the flat plate in the experiment, because So et al. (1999) have found that thickness has little or no effect on the response of the airfoil. Important flow parameters such as sv, Γ and the convection velocity U_c of the vortices were required as inputs for the numerical model. These parameters were determined from the KVS theory developed in Chen (1972). The inputs for the structural model were calculated from the data listed in Table 2. Fairly good agreement between the calculated and measured $(Y_p/D)_{\mathrm{rms}}$ at the mid-span of the flat plate was obtained when the leading edge of the plate was within the R_2 regime, i.e., $3<S/D<5$. At larger gap sizes, i.e., $S/D>5$, the discrepancy between calculated and measured $(Y_p/D)_{\mathrm{rms}}$ was very substantial and the difference was about 48% below the measured value. This large underestimation could be attributed to the fact that when the plate was in the regime R_1, i.e., $S/D>5$, and the two rows of KVS vortices were no longer parallel and organized. Consequently, the assumption of two parallel rows of KVS vortices was not applicable and the input parameters were not appropriate.

In order to verify the above conjecture, numerical analysis of the present experiments with the elastic NACA0012 airfoil was carried out using inputs of sv, Γ and U_c derived from measurements of the cylinder wake. The parameters of the oncoming vortical flow at various S/D were directly determined from the PIV measurements in the R_2 and R_1 regime. Vortex-induced vibrations with a shift in the release points of the two KVS vortex rows, x_s, were calculated. The calculation results are compared with the measured $(Y_a/D)_{\mathrm{rms}}$ in Fig. 18. The experimentally measured x_s in the modified cylinder wake is $x_s/d=\frac{1}{2}$. The agreement between the calculated and measured value is greatly improved in the R_2 and R_1 regime, with a maximum discrepancy amounting to only 8% of the measured value. Extremely good agreement is also obtained between the calculated and measured bending energy $(E_Y)_a$ (Fig. 18(b)). For all cases examined, the calculated $(E_Y)_a$ only yields a discrepancy with measurements of about 10% at most. The discrepancies between calculations and measurements in $(Y_p/D)_{\mathrm{rms}}$ and $(E_Y)_a$ could be attributed to viscous effects, 3-D flow effects,

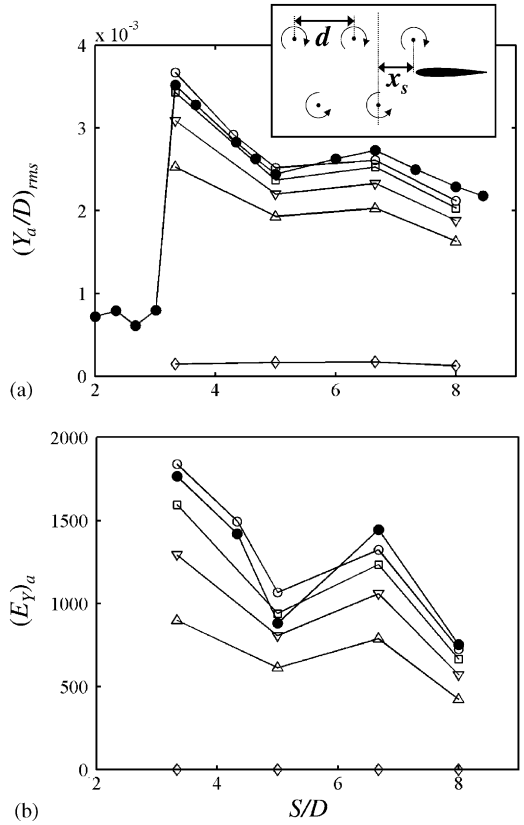

Fig. 18. Comparison of measured and calculated structural response of the airfoil: (a) rms bending amplitude; (b) bending energy. Numerical calculations: —○—, $x_s/d=\frac{1}{2}$; —□—, $x_s/d=\frac{1}{3}$; —▽—, $x_s/d=\frac{1}{4}$; —Δ—, $x_s/d=\frac{1}{6}$; —◇—, $x_s/d=0$. —●—, experimental measurements.

or uncertainty in the inflow parameters. This good agreement shows that the numerical model of So et al. (1999) is capable of estimating the vibration displacements and the associated energy transfer between the cylinder and the downstream airfoil or plate in the fluid–structure interaction problems considered, provided the input parameters such as sv, Γ and U_c are determined from measurements and not from the KVS theory.

References

Arai, N., Komatsu, M., 1992. Active control of the hydraulic forces of a body by a splitter plate. Computers and Fluids 21, 145–150.

Baban, F., So, R.M.C., 1991. Aspect ratio effect on flow-induced forces on circular cylinder in a cross-flow. Experiments in Fluids 10, 311–321.

Blake, W.K., 1986. Mechanics of Flow-Induced Sound and Vibration, vol. 1. Academic Press, New York.

Chen, Y.N., 1972. Fluctuating lift forces of the Karman vortex streets on single circular cylinders and in tube bundles. Part 1—The vortex street geometry of the single circular cylinder. *ASME* Journal of Engineering for Industry 94, 603–612.

Chen, S.S., 1987. Flow-Induced Vibration of Circular Cylindrical Structures. Hemisphere Publishing Corporation, Washington.

Fahy, F., 1985. Sound and Structural Vibration. Radiation, Transmission and Response. Academic Press, London, p. 65.

Gerrard, J.H., 1966. The mechanics of formation region of vortices behind bluff bodies. Journal of Fluid Mechanics 25, 401–413.

Hasan, M.A.Z., Budair, M.O., 1994. Role of splitter plates in modifying cylinder wake flows. AIAA Journal 32, 1992–1998.

Jadic, I., So, R.M.C., Mignolet, M.P., 1998. Analysis of fluid-structure interactions using a time marching technique. Journal of Fluids and Structures 12, 631–654.

Kawai, H., 1990. A discrete vortex analysis of flow around a vibrating cylinder with a splitter plate. Journal of Wind Engineering and Industrial Aerodynamics 35, 237–273.

Lakshmana Gowda, B.H., Prabhu, D.R., 1987. Interference effects on the flow-induced vibrations of a circular cylinder. Journal of Sound and Vibration 112, 487–502.

Lau, Y.L., 2003. Experimental and Numerical Studies of Fluid–Structure Interaction in Flow-Induced Vibration Problems. Ph.D. Thesis, Department of Mechanical Engineering, The Hong Kong Polytechnic University.

Lau, Y.L., So, R.M.C., Liu, Y., Leung, R.C.K., 2002. Validation of a two-dimensional numerical model for vortex/blade interaction. Proceedings of the Fifth International Symposium on Fluid–Structure Interactions, Aeroelasticity, Flow-Induced Vibration & Noise, IMECE2002-32223, New Orleans, LA, USA, November 17–22.

Lee, S.J., Kim, H.B., 1997. The effect of surface protrusions on the near wake of a circular cylinder. Journal of Wind Engineering and Industrial Aerodynamics 69-71, 351–361.

Leung, R.C.K., So, R.M.C., 2001. Noise generation of blade-vortex resonance. Journal of Sound and Vibration 245, 217–237.

Luk, K.F., So, R.M.C., Leung, R.C.K., Lau, Y.L., Kot, S.C., 2004. Aerodynamic and structural resonance of an elastic airfoil due to oncoming vortices. AIAA Journal 42, 899–907.

Lin, J.-C., Towfighi, J., Rockwell, D., 1995. Instantaneous structure of near-wake of a circular cylinder: on the effect of Reynolds number. Journal of Fluids and Structures 9, 409–418.

Lin, S.Y., Wu, T.M., 1994. Flow control simulations around a circular cylinder by a finite volume scheme. Numerical Heat Transfer 26, 301–319.

Mansingh, V., Oosthuizen, P.H., 1990. Effects of splitter plates on the wake flow behind a bluff body. AIAA Journal 28, 778–783.

Nakagawa, T., 1986. A formation mechanism of alternating vortices behind a circular cylinder at high Reynolds number. Journal of Wind Engineering and Industrial Aerodynamics 25, 113–129.

Nakagawa, T., 1988. On unsteady airfoil-vortex interaction. Acta Mechanica 75, 1–13.

Nakamura, Y., Tomonari, Y., 1977. Galloping of rectangular prisms in a smooth and in a turbulent flow. Journal of Sound and Vibration 52, 233–241.

Nakamura, Y., Hirata, K., Kashima, K., 1994. Galloping of a circular cylinder in the presence of a splitter plate. Journal of Fluids and Structures 8, 355–365.

Norberg, C., 2001. Flow around a circular cylinder: aspects of fluctuating lift. Journal of Fluids and Structures 15, 459–469.

Norberg, C., 2003. Fluctuating lift on a circular cylinder: review and new measurements. Journal of Fluids and Structures 17, 57–96.

Obara, H., Matsudaira, Y., 1998. Large vortex formation-mechanism behind wedge under several separation conditions. JSME International Journal Series B 41 (4), 788–795.

Ozono, S., 1999. Flow control of vortex shedding by a short splitter plate asymmetrically arranged downstream of a cylinder. Physics of Fluids 11, 2928–2934.

Perry, A.E., Chong, M.S., Lim, T.T., 1982. The vortex-shedding process behind two-dimensional bluff bodies. Journal of Fluid Mechanics 116, 77–90.

Pozrikidis, C., 1997. Introduction to Theoretical and Computational Fluid Dynamics. Oxford University Press, New York, pp.64–65

Roshko, A., 1955. On the wake and drag of bluff bodies. Journal of Aerospace Science 22, 124–132.

So, R.M.C., Jadic, I., Mignolet, M.P., 1999. Fluid-structure resonance produced by oncoming alternating vortices. Journal of Fluids and Structures 13, 519–548.

So, R.M.C., Zhou, Y., Liu, M.H., 2000. Free vibrations of an elastic cylinder in a cross flow and their effects on the near wake. Experiments in Fluids 29, 130–144.

So, R.M.C., Liu, Y., Chan, S.T., Lam, K., 2001. Numerical studies of a freely vibrating cylinder in a cross flow. Journal of Fluids and Structures 15, 845–866.

Streitlien, K., Triantafyllou, G.S., Triantafyllou, M.S., 1996. Efficient foil propulsion through vortex control. AIAA Journal 28, 222–228.

Unal, M.F., Rockwell, D., 1988. On vortex formation from a cylinder. Part 1. The initial instability. Journal of Fluid Mechanics 190, 491–512.

van Dyke, M., 1982. An Album of Fluid Motion. The Parabolic Press, Stanford, CA, USA.

Zdravkovich, M.M., 1985. Flow induced oscillations of two interfering circular cylinders. Journal of Sound and Vibration 101, 511–521.

Zdravkovich, M.M., 1997. Flow Around Circular Cylinders. Oxford University Press, New York, p. 121.

Zhou, Y., Wang, Z.J., So, R.M.C., Xu, S.J., Jin, W., 2001. Free vibration of two side-by-side cylinders in a cross flow. Journal of Fluid Mechanics 443, 197–229.